Meteoroid and Orbital Debris Threats to NASA's Docking Seals: Initial Assessment and Methodology

Henry C. de Groh III,[1] Christopher A. Gallo,[2] and Henry K. Nahra[3]
NASA Glenn Research Center, Cleveland, Ohio, 44135

The Crew Exploration Vehicle (CEV) will be exposed to the Micrometeoroid Orbital Debris (MMOD) environment in Low Earth Orbit (LEO) during missions to the International Space Station (ISS) and to the micrometeoroid environment during lunar missions. The CEV will be equipped with a docking system which enables it to connect to ISS and the lunar module known as Altair; this docking system includes a hatch that opens so crew and supplies can pass between the spacecrafts. This docking system is known as the Low Impact Docking System (LIDS) and uses a silicone rubber seal to seal in cabin air. The rubber seal on LIDS presses against a metal flange on ISS (or Altair). All of these mating surfaces are exposed to the space environment prior to docking. The effects of atomic oxygen, ultraviolet and ionizing radiation, and MMOD have been estimated using ground based facilities. This work presents an initial methodology to predict meteoroid and orbital debris threats to candidate docking seals being considered for LIDS. The methodology integrates the results of ground based hypervelocity impacts on silicone rubber seals and aluminum sheets, risk assessments of the MMOD environment for a variety of mission scenarios, and candidate failure criteria. The experimental effort that addressed the effects of projectile incidence angle, speed, mass, and density, relations between projectile size and resulting crater size, and relations between crater size and the leak rate of candidate seals has culminated in a definition of the seal/flange failure criteria. The risk assessment performed with the BUMPER code used the failure criteria to determine the probability of failure of the seal/flange system and compared the risk to the allotted risk dictated by NASA's program requirements.

Nomenclature

A	=	spacecraft surface area exposed to MMOD threats, m^2
c-c	=	distance between the center of the crater and the center-line of the seal, mm
D_{seal}	=	average diameter of the crater in the elastomer, = $(d_v + d_s + d_c)/3$, mm
D_f	=	average diameter of the crater in the flange material, in this case, aluminum alloy, = $(d_{fi} + d_{fo})/2$, mm
d_{fi}	=	average inner diameter of the crater, in plane with the surface of the metal target, mm
d_{fo}	=	average outer diameter of the crater, the outer diameter of the metal crater's crown, mm
d_v	=	average maximum diameter vaporized in the crater in the elastomer, mm
d_s	=	average diameter of secondary crater damage in the elastomer, mm
d_c	=	average diameter of radial cracks in the elastomer, mm
D_{crit}	=	the minimum crater diameter that causes seal or flange failure, the "critical" crater diameter, mm
h	=	crown height of the crater, mm
KE	=	kinetic energy, joules, J
m	=	projectile mass
P(Sio)	=	The intersection of failure probabilities for the inner and outer seals
P(SiFo)	=	The intersection of failure probabilities for the inner seal and outer flange area
P(SoFi)	=	The intersection of failure probabilities for the outer seal and inner flange area
P(Fio)	=	The intersection of failure probabilities for the inner and outer flange areas

[1] Materials Research Eng., Advanced Metallics Branch, NASA Glenn/M.S. 23-3, Cleveland OH.
[2] Aerospace Engineer, Systems Engineering Division, NASA Glenn/M.S. 86-1.
[3] Aerospace Eng./MMOD Service Module Lead, Fluids Systems Branch, NASA Glenn, 21,000 Brookpark Rd. Cleveland OH, AIAA Member Grade: Associate Fellow.

ρ_p = projectile density, g/cm^3
ρ_t = target density, g/cm^3
t = time exposed to MMOD threats, years
V = projectile impact velocity, km/s
w_{bulb} = width of the elastomer seal bulb, mm
W = width of the whole seal area being considered, mm
W_F = seal or flange width upon which a particular particle must hit to cause a failure; example for flange: $W_{F|f} = D_f - D_{crit|f}$, mm
s = as a subscript refers to the elastomer seal
f = as a subscript refers to the metal flange
F = as a subscript refers to seal/flange failure

Acronyms

APAS = Androgynous Peripheral Attachment System
ATLAS = APAS To Low impact docking system Adaptor System
BLE = Ballistic Limit Equation
C-P = Cour-Palais
CEV = Crew Exploration Vehicle
HVI = Hypervelocity Impact
ISS = International Space Station
LIDS = Low Impact Docking System
LOC = Loss of Crew
LOM = Loss of Mission
LOMo = Loss of Mission objective
MEM = Meteoroid Engineering Model
MMOD = Micrometeoroid and Orbital Debris
NASA = National Aeronautics and Space Administration
ORDEM = Orbital Debris Engineering Model
PNF = Probability of No Failure
PNP = Probability of No Penetration
POF = Probability of Failure
SRD = Systems Requirements Document
WSTF = White Sands Test Facility

I. Introduction

WHILE in space, NASA's Crew Exploration Vehicle (CEV) and the International Space Station (ISS) will be exposed to very high velocity impacts from space debris and meteoroids.[1-6] These threats are commonly referred to as Micrometeoroid Orbital Debris (MMOD). The CEV will have a docking system which enables it to connect to ISS and other spacecraft and a hatch that opens so crew and supplies can pass between them. This docking system is known as the Low Impact Docking System (LIDS) and uses a silicone rubber seal to seal in cabin air.[7] Figure 1 shows schematics of ISS, CEV, LIDS, and the LIDS main seal- which is a set of two concentric seals. The rubber seals on LIDS press against an aluminum flange on ISS. Prior to docking, both of these mating surfaces are exposed to the space environment. The level of environmental exposure received by an object like the seals depends primarily on the object's altitude and orientation relative to its orbital velocity vector, the Earth, and the Sun. The main aspects of the space environment that cause damage to spacecraft are atomic oxygen, ultraviolet and ionizing radiations, and MMOD.[8] The effects of atomic oxygen, ultraviolet and ionizing radiations on the LIDS seals have been presented elsewhere.[9]

The objective of this work is to determine the risk of LIDS seal failure due to MMOD threats and compare these expected risks to allowable risk specifications for various missions. Such an assessment involves hypervelocity impact (HVI) testing that leads to a well defined failure criteria which in turn, in conjunction with a risk analysis, enables expected risk levels to be compared to risk levels allowed for NASA missions. This paper presents our results of ground based hypervelocity impacts on silicone rubber seals and aluminum sheet plates along with an assessment of the MMOD environment posed risk relevant to a variety of CEV mission scenarios. The methodology developed also is used to evaluate different candidate seal designs and corresponding risk levels to help guide future design decisions.

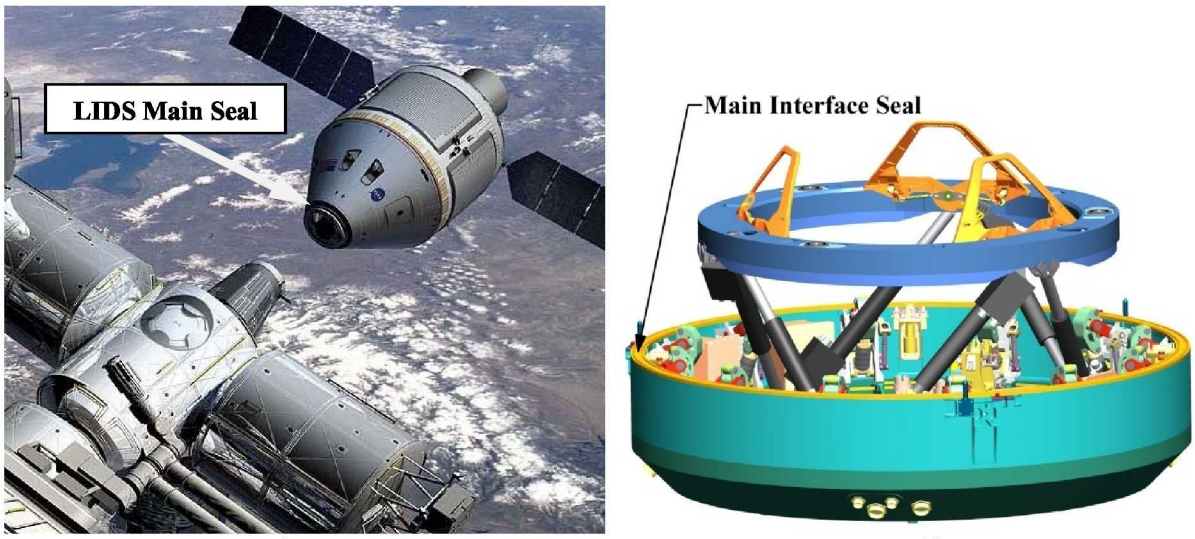

a) b)

Figure 1. ISS, CEV, LIDS and the LIDS seal. a) Artist's drawing of CEV docking to ISS; b) Schematic of LIDS and its primary seal which are located at the nose of CEV.

Although silicone based seals have been used extensively by NASA,[10] we have not found applicable hypervelocity impact studies for elastomers prior to the work presented here. Related work has typically concentrated on modeling the MMOD environment,[11-14] or on metal, glass, or composite targets, or on the depth of penetration of the hypervelocity projectile, rather than the diameter of the crater and characteristics of the crater's crown (the area around the crater that is raised above the surface of the substrate).[11,15-17] Many estimates of crater size or depth begin with Cour-Palais type relations.[11,12,15] which are applicable to the threshold penetration of single, thin, ductile metal plates. Cour-Palais relations in connection with penetration are not directly applicable to our case since we are considering elastomers instead of ductile metals, relatively thick targets, and have a failure mode that is dominated by the surface diameter of the crater and crown morphology, not by projectile penetration depth. Our seals generally fail one of three ways. The first failure mode is when the projectile makes a crater in the elastomer that spans the width of the seal. The second is when the diameter of the crater in the metal surface, upon which the seal is to mate, spans the width of the seal. The third failure mode is when the crown of the crater is very tall or has "rolled over" making a tube, or protected area, that the seal cannot seal over. The depth of projectile penetration found through Cour-Palais type data and analysis is not equal to the crater's diameter in-plane with the target's surface. However, prior work has shown that for projectiles and targets of the same material, at sufficiently high velocities, the in-plane diameter of a crater is close to two times the depth of the crater.[18,19] Cour-Palais estimates (with the adoption of this semi-spherical convention) and other scaling laws,[20] will be compared to recent hypervelocity tests in aluminum and silicone based elastomers.

Elastomer seals made of two silicone based elastomer compounds were impacted with hypervelocity particles. The compounds tested were Parker S0383-70 which has a durometer Shore A hardness of 70, and Esterline ELS-SA-401 which has a Shore A hardness of about 40. Due to limits on the clamping force applied when LIDS docks, the baseline seal made from the Parker compound is narrow compared to the softer Esterline seal, which is 9.1 mm wide. The leak rate of these seals was tested before and after impacts.

The LIDS seal mates to an aluminum alloy flange. To examine how the seals will perform with a flange that might be damaged from MMOD, 6 mm thick aluminum alloy plates were impacted, then an undamaged seal was placed over the impact crater and leak tested. In this way, the smallest particle (lowest kinetic energy) that would cause a seal failure was determined. With this information, the probability of impact by such a particle (or ones of greater kinetic energy) was determined using NASA sanctioned risk assessment codes which model the MMOD environment and the likelihood of impacts resulting from various mission scenario inputs.[4]

NASA has established a set of design specifications for the Constellation Program.[21] The design specifications relating to the MMOD environment are defined in Ref. 22, where it is stated that the orbital debris environment of LEO will be determined using the Orbital Debris Engineering Model 2000 (ORDEM2000) and the meteoroid environment will be determined using the Meteoroid Engineering Model (MEM). Mission parameters are input into

these two codes which then provide detailed solutions of MMOD flux and velocity. We use these environments and the code known as BUMPER to estimate the risks of LIDS seal failure due to hypervelocity impacts from MMOD.

The BUMPER computer code is a FORTRAN program that calculates the Probability of No Penetration (PNP) or Probability of No Impact (PNI) of a spacecraft structure. The BUMPER code version 1.48LM-G dated 09/26/2008 was used for this analysis. This version has been modified by Lockheed Martin for the Crew Exploration Vehicle (CEV) configuration. A finite element model of the object to be analyzed is generated by using either the I-DEAS or PATRAN graphics programs. The code reads in the node and element geometry of the model consisting of two dimensional shell elements. The shell elements have different protection geometries which allow penetration to begin at different critical particle diameters. The critical penetrating particle diameter is defined as a function of the impact velocity by the Ballistic Limit Equation (BLE) function. Then the ballistic limit function is selected along with the thicknesses and materials of the wall and shielding configuration. Once all the parameters of the model and walls have been entered into the code, the orbital debris model ORDEM2000 and the Meteoroid Engineering Model (MEM) are called to define the number of penetrating particles on each of the elements possessing a unique BLE that is based on the protection geometry, material properties and orientation. The determination of the number of impacts involves integration over the particle velocity distribution and directionality of MMOD. In the determination of the number of impacts, a particle diameter is usually specified and BUMPER predicts the number of impacts of this particle or larger. However, the determination of the number of penetrating particles involves an integration of the particle diameter which for penetration is a function of the velocity as given by the BLE equations. After the determination of the number of penetrating or impacting particles, the probability of no penetration is calculated for the selected element ranges of the model for either the orbital debris or the micro-meteoroid environments. Missions to ISS are in low earth orbits where significant MMOD threats from both debris and meteoroids exist. However, for lunar missions the orbital debris environment is relevant primarily for the mission duration spent in LEO; after earth departure, the micrometeoroid environment becomes more relevant for risk assessments of the vehicle.

We present in this paper under "II. Procedure" and in section A, the experiment procedures which encompass the target and projectile description, and the description of the HVI tests. In section B, we introduce the methods used in measuring the craters' parameters and characteristics like the diameter and crown height for the aluminum and elastomers. Section C briefly discusses the leakage tests aimed at defining the damaged seal/flange leak rates and thereby the failure criteria. Section D addresses the assumptions that went into the BUMPER risk assessment. Under "III Results", we present in section E the results of the crater diameter given as a function of the projectile kinetic energy from the experimental data for the damaged aluminum and elastomers. The results of the MMOD BUMPER code assessment are presented in section F where the results are compared to NASA risk requirements. The paper closes with the Conclusion section.

II. Procedure

A. Hypervelocity impacts

1. Targets

Hypervelocity impacts of elastomer and aluminum alloy targets were done at White Sands Test Facility in New Mexico by a team lead by Donald Henderson and Karen Rodriguez. The two peroxide cured, silicone based elastomer compounds were Parker's S0383-70, and Esterline's ELA-SA-401. Parker's S0383-70 is rust colored with a Shore A hardness of 70; Esterline's ELA-SA-401 is blond with a hardness of 40. The 6061-T651 aluminum targets were 178 x 178 x 6.35 mm thick (7 x 7 x ¼ in.) with a surface finish of 0.4 μm (15 microinches). Elastomer targets were tested in the "as received condition", and after a treatment of atomic oxygen. Atomic oxygen treatments are used to form a SiO_x rich surface layer to decrease the adhesive properties of the elastomers.[23] Aluminum targets were tested as received, anodized (MIL-A-8625, Type II, Class 1), and after receiving a 0.013 mm (0.0005 in.) thick coating of electroless nickel (AMS-C-26074, Class 4, Grade A). It is expected that the flanges on ISS to which LIDS will mate will be aluminum alloy, either anodized, or perhaps coated with nickel for electrical conductivity reasons.

Two basic LIDS seal designs are being examined, both are double seals, the Parker seal, known as a Gask-O-Seal, is relatively narrow while the Esterline seal, known as Esterline/NASA 2-piece seal, is able to be wider since it is softer. A wider seal is more resistant to MMOD, however also causes clamping loads to increase; the width of the seal is limited by its hardness and allowable clamping loads. Figure 2 shows scaled down versions of the LIDS seals we are testing, and schematics of their cross sections. In hypervelocity tests, the LIDS seal designs were mimicked using seals of similar cross section cut from 5.5 mm thick sheet material of the same elastomer compound using a water-knife. We are in the process now of impacting small scale engineering seals. Figure 3 shows examples of the seals used in this study. In addition to these, a couple tests impacted a 3.2 mm (1/8 in.) thick aluminum plate coated

with a 0.51 mm thick layer of the Parker S0383-70 compound simulating the web material at the base of the Gask-O-Seal trough. The layer of elastomer was bonded to the plate by Parker using the same methods they use in the production of Gask-O-Seals.

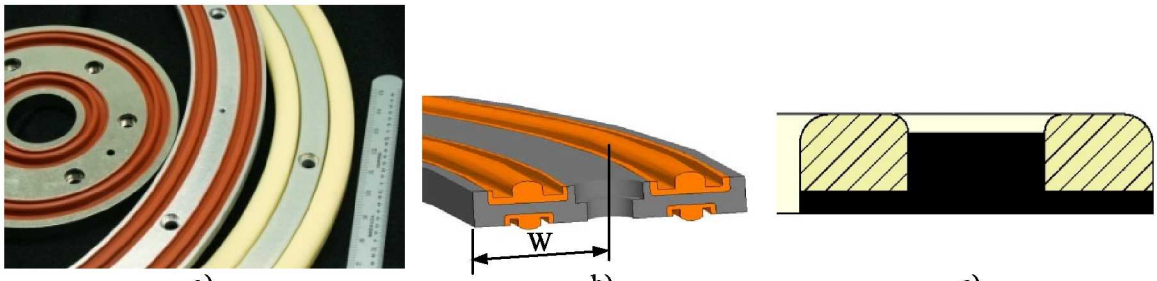

a) b) c)

Figure 2. Parker Gask-O-Seal, and Esterline/NASA 2-piece seal. a) 10 cm diameter Parker seal, 30.5 cm diameter Parker seal, and the Esterline seal with 9.1 mm wide seal beads (blond); b) schematic of the Parker Gask-O-Seal cross section with the width of the inner seal area, W, shown; c) schematic of the Esterline seal.

a) b) c)

Figure 3. Test articles used in hypervelocity impact tests. a) 5.2 mm and 2.5 mm wide Parker "ring" seals; b) 9.1 mm wide Esterline "ring" seal; c) anodized aluminum plate cratered by a 1 mm diameter, 1.4 mg, 8 km/s aluminum projectile and a 5.1 mm wide Parker seal.

2. Projectiles

The space environment is populated with meteoroids and debris. Debris is prevalent in LEO, but decreases as orbital altitude increases. The average velocity of debris is between 7 and 8 km/s for particles between 0.01 and 1 cm respectively. The average velocity of meteoroids is about 20 km/s.[11,24] The density of orbital debris varies, but a good approximation of the average density of debris is 2.7 g/cm^3, the density of aluminum.[13,24] Although rocky and iron rich meteoroids exist, meteoroids are primarily made of ice. Thus a density of 1 g/cm^3 is considered a good estimate of meteoroid density.[22] The velocities characteristic of meteoroids exceed current ground based hypervelocity impact capabilities. However, velocities characteristic of debris (7.5 km/s) can be well matched by facilities at White Sands Test Facility (WSTF). Densities of projectiles can also be well matched in labs. Three different materials were used as projectiles, all were in the form of spheres: 2017 T4 grade 200 aluminum, density = 2.79 g/cm^3, hardness 105 HB; dry soda lime glass, density = 2.5 g/ cm^3; and Nylon66, density = 1.14 g/ cm^3.

3. Hypervelocity Impacts

Hypervelocity impacts were performed at the White Sands Test Facility (WSTF) Remote Hypervelocity Test Laboratory (RHTL) in Las Cruces, New Mexico using their .17-caliber Light Gas Gun.[25] This system verifies the condition of the projectile and measures particle velocity using ultra-high speed digital imaging SIM cameras manufactured by Photo-Sonics. Projectile velocity is also measured with laser intervalometer and photodiode flash detectors. Maximum velocities available were about 8.3 km/s; tests at between 5 and 8.3 km/s were done. The velocity goal for most tests was 8.2 km/s. Most impacts were done at room temperature; a small group of impacts were done near -78 °C (-105 °F); a few tests are planned at the maximum LIDS seal temperature expected of 125 °C (257 °F). The direction, or angle, of the incoming projectile was set at 0°, 45°, or 60°, where 0° is coming straight in, perpendicular to the target's surface. Impacts done at an angle were set up such that the path of the projectile was parallel to the seal's major radius, coming from the seal's center, towards its outer diameter. Most tests were done at 0° due to the difficulty of hitting the seal, especially the narrow Parker seals, when turned at an angle.

Table 1 presents the hypervelocity tests accomplished and used in this study to determine crater diameters and seal failures resulting from various projectiles. The Strike # and Specimen ID are included to assist with traceability.

Table 1. Projectiles, targets and velocities used in impact tests. Targets were Parker S0383-70, Esterline ELA-SA-401, 6061 T651 aluminum, or the aluminum coated with a 0.51 mm thick layer of the Parker elastomer. Pre-treatment notes exposure to atomic oxygen, or a coating on the aluminum. Mass was calculated based on density and diameter. All projectiles were spherical. Aluminum projectiles were 2017 T4 grade 200 ball bearings, ρ_p = 2.79 g/cm^3; Glass projectiles were 9000 Series soda lime glass size standards, ρ_p =2.5 g/cm^3; Nylon 66 had a density of 1.14 g/cm^3; the steel projectile was 440 C stainless, ρ_p =7.7 g/cm^3. Strikes 35c, 35d, and 37 were done with the target cooled to -78 °C (-108 °F).

Strike #	Target material	Target AO Treatment atoms/cm^2, or coating	Target width or thickness, mm	Angle, degrees off vertical	Mass, mg	Projectile diameter, mm	Projectile Density, g/cc	Velocity, km/s
31	Parker	As Received	2.5 wide	0	0.093	0.4	2.79	7.57
29	Parker	8.0E+19	2.5 wide	0	0.093	0.4	2.79	5.75
9	Parker	8.0E+19	2.5 wide	0	0.084	0.4	2.52	8.19
35c	Parker (-78 °C)	1.0E+20	2.5 wide	0	0.093	0.4	2.79	7.8
17	Parker	1.0E+20	2.5 wide	45	0.093	0.4	2.79	7.93
35d	Parker (-78 °C)	1.2E+20	2.5 wide	0	0.093	0.4	2.79	8.22
15	Parker	1.0E+20	2.5 wide	0	0.183	0.5	2.79	8.04
37	Parker (-78 °C)	1.2E+20	2.5 wide	0	0.183	0.5	2.79	8.29
6	Parker	8.0E+19	2.5 wide	0	0.316	0.6	2.79	8.22
6b	Parker	8.0E+19	2.5 wide	0	0.316	0.6	2.79	8.26
2	Parker	7.5E+20	5.2 wide	0	0.501	0.7	2.79	8.17
7d	Parker	3.5E+20	5.2 wide	60	0.748	0.8	2.79	8.27
7c	Parker	7.5E+20	5.2 wide	60	0.748	0.8	2.79	8.29
7f	Parker	3.5E+20	5.2 wide	60	0.805	0.82	2.79	8.24
21	Parker/Al	As Received	0.5 on 3 thick	0	0.093	0.4	2.79	8.24
22	Parker/Al	As Received	0.5 on 3 thick	60	0.748	0.8	2.79	8.19
30	Esterline	As Received	9.1 wide	0	1.461	1	2.79	5.56
32	Esterline	As Received	9.1 wide	0	1.461	1	2.79	7.47
5b	Esterline	As Received	9.1 wide	45	7.177	1.7	2.79	8.1
3	Esterline	3.4E+20	9.1 wide	60	0.501	0.7	2.79	8.21
1	Esterline	7.0E+20	9.1 wide	0	0.748	0.8	2.79	8.3
18	Esterline	1.0E+20	9.1 wide	0	1.031	1.2	1.14	7.84
36	Esterline	1.5E+20	9.1 wide	0	1.461	1	2.79	7.56
10	Esterline	1.0E+20	9.1 wide	0	1.319	1	2.52	8.38
4c	Esterline	3.4E+20	9.1 wide	0	1.461	1	2.79	8.19
16	Esterline	1.0E+20	9.1 wide	0	2.096	1.52	1.14	7.61
38b	Esterline	1.5E+20	9.1 wide	45	3.209	1.3	2.79	7.95
8c	Esterline	7.0E+20	9.1 wide	45	3.209	1.3	2.79	8.24
14	Al	As Received	6.3 thick	0	0.093	0.4	2.79	7.96
23	Al	As Received	6.3 thick	0	5.984	1.6	2.79	7.9
13	Al	Anodized	6.3 thick	0	0.183	0.5	2.79	8.14
12	Al	Anodized	6.3 thick	0	1.461	1	2.79	8.03
19	Al	Anodized	6.3 thick	0	5.762	1.58	2.79	7.9
11	Al	Anodized	6.3 thick	0	11.687	2	2.79	7.65
40	Al	Ni coated	6.3 thick	45	0.093	0.4	2.79	7.5
39b	Al	Ni coated	6.3 thick	0	0.093	0.4	2.79	8.34
50	Stainless	As Received	3.0 thick	0	0.504	0.5	7.7	7.6

The mass of the projectile provided was calculated based on the shape (spherical), diameter, and density of the particle. The diameter of the glass projectiles is accurate to within better than +/- 5% based on the certified mean diameters provided by the manufacturers of the spheres used.[26] The densities of the projectiles were taken from the literature for the aluminum and Nylon66 projectiles, and from the supplier of the glass spheres. The density of the soda lime glass used was 2.5 +/- 0.1 g/cm^3. The density of the 2017 T4 aluminum alloy used was 2.79 g/cm^3; variations in the copper content of this alloy can be expected to cause density variation of about +/- 1%. We have assumed a similar uncertainty, +/- 1%, in density for the Nylon projectiles.

B. Crater measurements and W_F

4. Crater measurements

Several measurements of damaged areas in the elastomer and aluminum alloy targets were made. From these measurements an average crater diameter, D_{seal} or D_f, was calculated. If the crater was elliptical, the diameter was set to the arithmetic average of the ellipse's major and minor axes.

For the elastomers, five measurements were made:

1) d_v: The average maximum diameter of the vaporized void at the center of the crater. An example of a crater in one of the elastomers tested is provided in Figure 4. It can be seen in the cross sectional view made by computed tomography (CT) provided in Figure 4 b) that the maximum diameter of the vaporized void is, in this case, larger than the entry hole. d_v was measured using optical photographs and close inspection of the crater and the level of undercutting. Figure 5 shows d_v drawn on a crater in a Parker seal.

2) d_{min}: The average minimum diameter of the crater, sometimes referred to as the entry hole.

3) d_s: The average diameter of secondary damage, such as a region, or secondary crater, created by chunks of the surface being blown off, as show in Figure 5. If there was no significant secondary damage, or if its diameter was less than d_v, d_s was set equal to d_v. For example, there is no significant secondary damage in the Esterline seal shown in Figure 4; in this case, d_s would be set equal to d_v.

4) d_c: The average diameter of the cracked region, as shown in Figures 4 and 5.

The average diameter of the crater in the elastomer, D_{seal}, was defined as the average of d_v, d_s, and d_c i.e. ($D_{seal} = (d_v + d_s + d_c)/3$).

5) The hit location of the projectile was quantified and defined by the surface distance between the crater's center and the center-line of the seal, c-c, (where the center-line of the seal is defined as the circumferential line midway between the seal's inner and outer diameters). This distance between the crater's center and seal's center-line, c-c, is also used in the testing of undamaged seals over cratered metal targets. Values of c-c are negative if the crater is closer to the seal's inner wall, positive if the crater is located nearer the outer wall of the seal, and c-c = 0 if the center of the crater is at the seal's center-line.

For the metal targets, three measurements were made:

1) d_{fi}: The average inner diameter of the metal crater. This measurement was taken from an image of the crater by placing a circle (or ellipse) around the crater near its inflection point, near where the crater meets the plane of the target's surface, as shown in Figure 6.

2) d_{fo}: The average outer diameter of the metal crater. This measurement was taken from an image of the crater by placing a circle (or ellipse) around the outer edges of the crater's crown, as shown in Figure 6.

3) h: The average height of the crown of the crater above the target's surface. Several measurements were taken of the height of the crater around is circumference and averaged. Measurements were made using a side view image of the crater with a scale placed near the crown.

The average crater diameter in metal targets, D_f, was the average of d_{fi} and d_{fo} i.e. ($D_f = (d_{fi} + d_{fo})/2$).

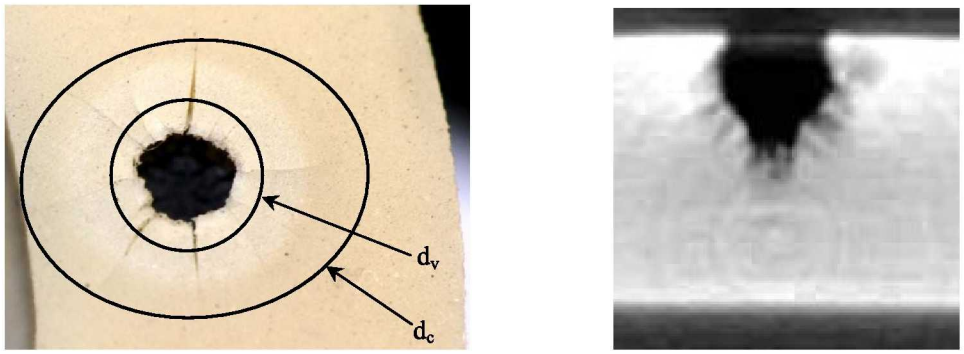

a) b)

Figure 4. Cratered Esterline seal. a) Top view of the 9.1 mm wide Esterline seal damaged by a 0.8 mm diameter, 0.728 mg Al sphere at 8.3 km/s, Strike 1; the black ellipses show d_c - the extent of cracks radiating from the crater, and d_v – the diameter of the vaporized material; b) Cross sectional view of the crater using computed tomography, seal is 5.5 mm thick, Strike 1.

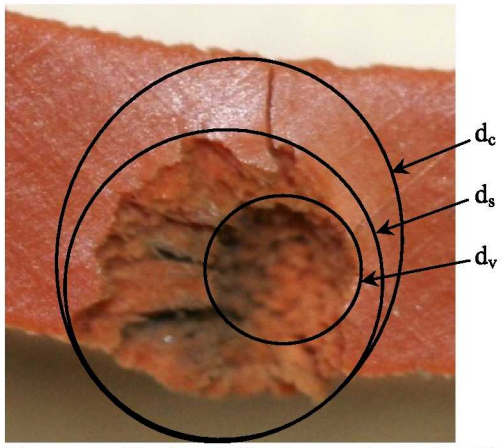

Figure 5. Cratered Parker seal. Strike 17, Parker 2.5 mm wide seal, hit by a 0.4 mm diameter, 0.093 mg aluminum sphere at 7.93 km/s, with the crater diameters d_v, d_s, and d_c shown.

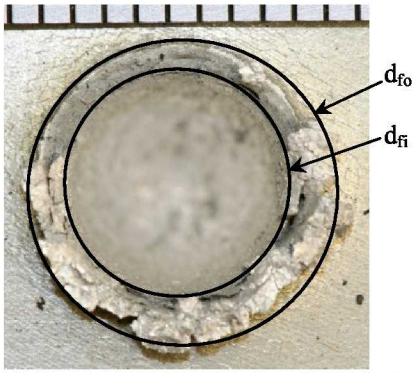

Figure 6. Cratered aluminum plate. Strike 19, the crater in an anodized 6061 T651 aluminum alloy plate resulting from a hit by a 1.58 mm diameter, 5.76 mg, aluminum sphere at 7.9 km/s; the black circles show the inner diameter, d_{fi}, and the outer diameter, d_{fo}; a mm scale is at the top of the image.

5. W_F, the seal/flange failure width

In this work, one of our goals is to determine the likelihood of a seal/flange failure. The likelihood of failure for our seals depends on the LIDS seal, the flange to which the seal mates, and the environment. We determine the probability of impact by various particles using the computer code known as BUMPER, BUMPER uses two programs, Orbital Debris Model-ORDEM2000 and Meteoroids Engineering Model-MEM to define the orbital debris and micrometeoroids environments and computes impinging particle fluxes. BUMPER computes the number of impacts or penetrations on a particular spacecraft area from MMOD taking surface directionality into consideration. A given area normally has a particular failure criteria applied to it. BUMPER considers the particle fluxes and failure criteria and determines the number of particles that will cause failure. The problem with applying this to the LIDS seal is that seal failure depends on the location of impact, thus the seal's failure criteria is not constant over its width. The weighting factor W_F/W is developed to proportion BUMPER results so that the sensitivity of the seal/flange area to impact location is accounted for.

The critical particle is defined as the particle with the lowest kinetic energy that will cause a seal or flange failure. The critical particle will cause a failure if it hits the seal (or flange) on the exact center-line of the seal only because if a critical particle hits the seal bulb a bit off center, only one of the side-walls blows out. Tests have shown only a small amount of side-wall is needed to prevent seal failure. If a critical particle hits off center on the flange, part of the seal will miss the crater and seal on the side farther from the crater. The larger the crater is, the further

from the center-line it can be and still cause a failure. This sensitivity of failure to crater size and hit location is brought into our analysis with the use of W_F, the width on the seal (or flange) upon which a particular crater must occur to cause failure. W_F is simply defined geometrically as the difference between the average crater diameter and the minimum average crater diameter that causes failure, as shown below with the subscripts f standing for the flange and s for the seal.

$$W_{F|s} = D_{Seal} - D_{Crit|s}$$
$$W_{F|f} = D_f - D_{Crit|f}$$

The two concentric LIDS seals are mounted to a flange that is 38.1 mm wide around the leading edge of the LIDS tunnel (Figures 1 and 2). It is our job to insure MMOD threats to this area are considered. To do this we divided this 38.1 mm width equally between the two seals so that the area we are including in our analysis of MMOD threats is 19.05 mm wide for each seal. This defines W for this work, where W is the effective "width of the seal" being considered in the MMOD analysis. W is the width of the elastomer seal plus areas immediately adjacent to the seal we are responsible for, since hits in these areas might also cause seal failure (Figure 2). This definition of area also defines limits to W_F which is thus bounded between 0 and 19.05 mm (the maximum width of the seal area being considered).

MMOD threats to the whole seal area are determined using BUMPER. These threats are weighted using the ratio W_F/W, thereby including the sensitivity of seal failure to hit location. For example, a particle that creates a crater of diameter D_{crit} will cause a seal failure if it strikes exactly on the seal's center-line. BUMPER is used to determine the likelihood of getting hit by such a critical particle anywhere in the area being considered (W wide). Normally getting hit by this critical particle would be considered a failure (or penetration) however the effective area at risk is zero because the critical particle must hit the exact center-line to cause failure, and since the center-line is infinitely narrow, the likelihood of hitting it is negligible (W_F and thus W_f/W go to 0). We multiply the probability of failure results that come from BUMPER for a particular kinetic energy by W_F/W. This ratio is 0 when the crater's surface diameter (D_f or D_{Seal}) is equal to or smaller than D_{crit}, and 1 when W_F is equal to or greater than W (19.05 mm in this case). In this way the sensitivity of seal failure to where the projectile hits in the seal area is included.

W_F and its ratio with W do not account for any effects related to damage mechanics. The damage done to the seal (D_{Seal}) is also dependent on hit location, with a maximum in damage occurring near the seal's center-line. Relations between the level of damage and hit location are beyond the scope of this paper, are currently being investigated, and will be discussed a later paper.[27] At this time, for conservatism, this seal damage maximum is assumed for all impacts.

C. Seal Leakage

Elastomer seals and aluminum alloy plates damaged by hypervelocity projectiles were leak tested in a fixture known as the Impact Specimen Flow Fixture.[28] Seals were compressed between flat plates 25% of their height and the space between them pressurized to 1 atm. above the pressure in the room. After pressurization input valves were closed and the system monitored for leakage via a pressure decay method with accurate pressure and temperature measurements. In the testing of cratered aluminum plates, an undamaged seal was used and the crater placed at various locations across the width of the seal. The details of seal leakage measurements and results are too extensive to be included here; these are being presented in another paper.[27] Some seal leakage data is included here however since it is an important factor in determining seal failure, and thus MMOD threats. Seals and plates were hit with particles of various kinetic energies, and then leak tested. In this way D_{crit} and the minimum kinetic energy required to cause seal failure was found for four cases: damaged Parker and Esterline seals against undamaged aluminum, and damaged aluminum pressed against undamaged Parker and Esterline seals. A seal/flange failure was defined as leakage equal to or greater than 0.001 kg air/day.

D. Risk Assessments using BUMPER

In the BUMPER risk assessment, the cumulative number of MMOD impacts of a particular kinetic energy or greater was determined. Below are the input boundary conditions used in the BUMPER risk assessments:

- Altitude – 400 km and 192,200 km
- Orbit inclination – 51.65° which is the orbital inclination of ISS.
- Year exposure starts: 2014.

- Time frames:
  - 4 days at 400 km: Conservative estimate of time for CEV to pursue and dock to ISS in LEO.
  - 8 days at 400 km: Estimate of time Altair is in LEO prior to docking with CEV.
  - 1, 2, 5, and 10 years at 400 km: Various times the ISS side of LIDS (ATLAS) might be exposed to LEO prior to docking with CEV.
  - 217 days at 192,200 km: Estimate of time in lunar orbit during a Lunar Outpost mission.

  These time frames were used to build scenarios of missions to ISS, Lunar Sortie, and Lunar Outpost.
- When the vehicle is in LEO, MEMCxPv2 is used to predict the micrometeoroid flux and ORDEM2000 to predict the orbital debris flux. When in lunar orbit, LunarMEMv2 is used for flux calculation.
- Area – The inner and outer seal areas were considered 2-D, defined by the following inner and outer areas: Inner seal area = 0.08475 m^2, Outer seal area = 0.08703 m^2.
- Orientation: For conservatism, seal and flange areas were assumed to be facing into the orbital velocity vector.
- Impact angle cut off – 89°.
- Density =$\rho_{p|MM}$ = 1g/cc where MM stands for micrometeoroid.
- Density =$\rho_{p|OD}$ = 2.7g/cm^3 where OD stands for orbital debris.
- Elastomer Yield Strength – Tensile Strength = UTS = 1050 psi.
- Speed of sound in silicone rubber = 984 m/s (3280 ft/s); in 6061 aluminum = 6400 m/s (21,000 ft/s).
- Brinell Hardness – Elastomers typically use the Shore A durometer scale for hardness. Esterline's ELA-SA-401 has a Shore A (SA) hardness of 38, Parker's S0383-70 has a SA hardness of 70; these are approximately equivalent to 9 and 15 BH respectively. Over aged 6061 T651 aluminum ~ 70 HB.
- Kinetic Energy – KE inputs for the Parker seal design were between 2 and 2000 Joules; Inputs for cases using the Esterline design were between 200 and 16,000 J.

In these simulations we used a function within BUMPER known as Option 41 when prompted for a penetration function, and failure criteria for a semi-infinite plate. By specifying the kinetic energy through Option 41, the diameter is expressed in terms of the velocity and such an expression is used as the BLE in BUMPER. We used the RESPONSE function from the main menu to build a .rsp table using the ballistic limit equation in Option 41. Using a result type request of "number of penetrations" the SHIELD option within BUMPER calculates the number of impacts at the given kinetic energy.

III. Results

E. Crater Size and Seal Failure

Measurements made on damaged plates and seals are presented in Tables 2, 3, and 4. The maximum leakage allowed for the whole CEV spacecraft is about 0.01 kg air/day. The maximum leakage allocated for the LIDS seal is about 0.001 kg air/day. We chose this as the leakage failure criteria corresponding to a Loss of Mission objective. Table 2 presents results for 6061 aluminum plates, listing the Strike number, the mass, velocity, and kinetic energy of the particle that hit the plate, the inner (d_{fi}), outer (d_{fo}) and average diameter of the crater (D_f), the crater's crown height, h, and whether or not a seal was able to seal over the crater. Based on these results, it is concluded that an undamaged 2.5 mm wide Parker seal will not be able to seal over a crater in aluminum made by a particle with kinetic energy of 2.9 joules. The 9.1 mm wide Esterline seal fails over craters made by particles of about 180 joules kinetic energy. The energies at which the seals fail are important observations that enable us to determine the crater diameter that causes seal failure, D_{crit}, and W_F. Strike 23 provides an example of some of the complexities of seal failure. There is a peak in the crown height near 180 J (Strike 19) for impacts such as these into aluminum; at this kinetic energy, the crater's crown is most full and intact and causes the leakage failure for this particular Esterline seal. At energies greater than 180 J the crown height declined; parts of the crown appeared to get blown off and the seal did not fail (Strike 23). As kinetic energy is raised further, the crater diameter increase and causes failure, as seen in Strike 11. In our analysis of the Esterline seal, we assume all impacts equal to or greater than 180 J cause seal failure. Note also that the Parker seal did not fail when placed over the crater produced in Strike 39b, even though it did fail over the crater of Strike 14, which was less energetic than Strike 39b. This might be due in part to the nickel coating on the target of Strike 39b; the target in Strike 14 was as received thus was not nickel coated or anodized.

Table 2. Surface Diameters of Craters in Flange Materials. Leakage column indicates seal pass or failure for the 2.5 mm wide Parker seal (P), or the 9.1 mm wide Esterline (E) seal. All targets were 6061 T651 aluminum except for Strike 50, which was stainless steel. Seal failure is defined as leakage > 0.001 kg air/day. See Table 1 for additional Strike details such as projectile density, and incoming angle.

Strike #	Mass, mg	Velocity, km/s	Kinetic Energy, Joules	Crater ID, d_{fi}, mm	Crater OD, d_{fo}, mm	Ave. Crater dia., D_f, mm	Crown Height, h, mm	Leakage
40	0.093	7.5	2.63	1.46	1.73	1.59	0.255	P-Pass
14	0.093	7.96	2.96	1.78	2.47	2.13	0.351	P-Fail
39b	0.093	8.34	3.25	1.75	2.20	1.98	0.344	P-Pass
13	0.183	8.14	6.05	2.20	2.82	2.51	0.42	P-Fail
12	1.461	8.03	47.10	4.70	6.10	5.40	0.98	E-Pass
19	5.762	7.9	179.80	7.02	9.57	8.30	1.50	E-Fail
23	5.984	7.9	186.72	7.09	9.29	8.19	1.27	E-Pass
11	11.687	7.65	341.97	9.30	10.80	10.05	1.00	E-Fail
50	0.504	7.6	14.55	1.96	2.67	2.32		

Table 3. Surface Diameters for Craters in Parker's S0383-70 elastomer. Kinetic energy is calculated using the projectile velocity, not the velocity component perpendicular to the target. Strikes 2 and 7, boxed in bold, used wider Parker seals (5.2 mm), Strikes 21 and 22 were on large aluminum plates with a 0.5 mm thick coating of S0383-70, all other strikes were on 2.5 mm wide seals. See Table 1 for additional details on specific Strikes. The accuracy of leakage flow measurements was typically +/- 5 x 10^{-6} kg air/day, thus leakage below this level is listed as 5 x 10^{-6} kg/day. Seal failure is defined as leakage > 0.001 kg air/day. Shaded data was used in Figure 8 and in the calculation of the $D_{seal}(KE)$ power law function. Strikes 35c, d, and 37 were at -78 °C.

Strike #	Mass mg	Velocity km/s	Kinetic Energy Joules	d_v mm	d_s mm	d_c mm	Ave. Crater dia., D_{seal} mm	Distance from seal's center c-c mm	Leakage kg air/day
29	0.093	5.75	1.55	1.07	1.89	2.6	1.853	0.18	5.0E-06
31	0.093	7.57	2.68	0.68	0.972	1.08	0.911	-1.06	5.0E-06
9	0.084	8.19	2.83	1.275	2.196	2.84	2.104	0.041	0.02
35c	0.093	7.8	2.84	1.17	1.544	1.717	1.477	0.94	5.0E-06
17	0.093	7.93	2.94	1.14	2.44	2.8	2.127	0.38	5.0E-06
35d	0.093	8.22	3.16	1.125	1.63	1.76	1.505	-0.69	5.0E-06
15	0.183	8.04	5.90	1.52	3.26	3.38	2.720	-0.19	0.3
37	0.183	8.29	6.27	1.86	3.27	3.36	2.830	-0.3	0.1
6	0.316	8.22	10.66	1.105	1.31	1.91	1.442	1.02	5.4E-06
6b	0.316	8.26	10.76	1.89	4.01	4.07	3.323	0.167	0.2
2	0.501	8.17	16.72	2.37	4.69	6.43	4.497	-0.4	5.0E-06
7d	0.748	8.27	25.58	3.06	4.52	7.75	5.110	n/a	5.0E-06
7c	0.748	8.29	25.70	1.96	3.45	3.93	3.113	1.83	5.0E-06
7f	0.805	8.24	27.34	2.46	5.27	6.2	4.643	n/a	5.0E-06
21	0.093	8.24	3.17	2.4	2.75	2.98	2.710	n/a	
22	0.748	8.19	25.08	3.45	6	6.2	5.217	n/a	

Table 4. Surface Diameters for Craters in Esterline's ELA-SA-401 elastomer. Kinetic energy is calculated using the projectile velocity, not the velocity component perpendicular to the target. See Table 1 for additional details on specific Strikes. The accuracy of leakage flow measurements was typically +/- 5 x 10^{-6} kg air/day, thus leakage below this level is listed as 5 x 10^{-6} kg/day. Seal failure is defined as leakage > 0.001 kg air/day. Strikes shaded gray were used in D_{seal}, KE power law analysis (Figure 7); Strikes 36 and 38b were at -78 C.

Strike #	Mass mg	Velocity km/s	Kinetic Energy Joules	dv mm	ds mm	dc mm	Ave. Crater dia., D_{seal} mm	Distance from seal's center, c-c mm	Leakage kg/day
3	0.501	8.21	16.887	2.95	4.506	4.81	4.09	2.3	5.0E-06
30	1.461	5.56	22.58	2.84	2.84	6.85	4.18	0.54	5.0E-06
1	0.748	8.3	25.763	3.29	3.29	6.6	4.39	-1.01	5.0E-06
18	1.031	7.84	31.699	3.45	6.09	7.81	5.78	2.06	5.0E-06
32	1.461	7.47	40.758	3.61	3.914	6.78	4.77	2.14	5.0E-06
36	1.461	7.56	41.746	3.2	3.2	4.89	3.76	3.37	5.0E-06
10	1.319	8.38	46.33	3.18	4.78	10.07	6.01	0.7	
4c	1.461	8.19	48.994	4.53	4.53	10.38	6.48	0	5.0E-06
16	2.096	7.61	60.698	4.23	8.49	10.12	7.61	0.187	0.3
38b	3.209	7.95	101.42	5.3	7.5	8.6	7.13	1.95	5.0E-06
8c	3.209	8.24	108.96	5.2	8.7	10.87	8.26	1.8	5.0E-06
5b	7.177	8.1	235.45	5.63	11.03	14.62	10.43	-0.63	0.3

Figure 7 shows the kinetic energy plotted with the resulting average crater diameter, D_f, for hits into aluminum targets. Note that kinetic energy in Table 2, and in the plot is calculated using the velocity of the particle, not the velocity component perpendicular to the target. A power law fit of these data yields the following:

$$D_f = 1.3(KE)^{0.3556} \quad (1)$$

where D_f is the average surface diameter of the crater in aluminum in units of mm, and KE is kinetic energy of the projectile in units of joules. We use Eq.(1) to determine D_f for each kinetic energy input into BUMPER. For each KE input, we can now find W_F (where $W_F = D_f - D_{crit}$) and the weighting ratio W_F/W. It is understood that it is unlikely that a particular HVI test will yield the exact KE_{crit}, and that the true KE_{crit} will likely be between a pair of tests conditions. The D_{crit} used to calculate W_F can be calculated from Eq.(1) by inputting an estimated KE_{crit} or from experimental measurements of crater diameters from tests which employed impact energies near KE_{crit}. We estimated KE_{crit} for each case based on the values in the tables, then used Eq.(1), (2), and (3) to determine the D_{crit} values used in the determination of W_F.

Consideration of crater size as a function of kinetic energy is more complicated when considering the elastomer seals compared to the semi-infinite flange materials. The level of damage done to the seal is dependent on where on the seal the projectile strikes. If the particle misses the seal, no damage is done; if the particle hits near an edge, close to the inner or outer side wall, the high pressure that develops on impact is relieved due to the hit's close proximity to the side wall. An example of this is provided by Strikes 6 and 6b (Table 3). Strike 6 hit near the side wall, about 1mm from the seal's center-line, caused a crater 1.4 mm wide, and did not cause a failure. Strike 6b had the same kinetic energy but hit near the seal's centerline (c-c = 0.167 mm), created a crater 3.3 mm wide, and caused a seal failure. Results to date show that target temperature influences damage. In our tests lower temperatures appear to slightly decrease damage in the elastomers. We have tests at elevated temperatures planned. Results from tests at low temperatures and hits near seal side walls were omitted when considering crater size as a function of projectile kinetic energy. Table 3 shows the tests included in Figure 8, shaded gray, and used to determine the power law function for the Parker elastomer:

$$D_{seal} = 1.476KE^{0.366} \quad (2).$$

The leakage data in Table 3 indicate that the minimum kinetic energy required to cause a seal failure is about 2.8 J for the 2.5 mm wide Parker seal. This KE_{crit} value is used with Eq.(2) to determine D_{crit} and W_F. The KE_{crit} value for Esterline seal failure distilled from Table 4 is 60 J.

The shaded gray data in Table 4 are presented in Figure 9 which shows the power law function found for the Esterline elastomer:

$$D_{seal} = 1.336KE^{0.3878} \qquad (3).$$

The filled triangles in Figure 9 are results from impacts using Nylon66 projectiles and show the limits of using kinetic energy in relation to crater diameter. Kinetic energy might relate well to aspects of hypervelocity impact damage, such as depth of penetration, however, we are interested in how the damage interacts with the LIDS seal, thus need to solve for damage aspects near the surface of the target because it is these surface aspects, like surface crater diameter, which cause seal failure. Particles of relatively low density yield larger than expected crater diameters when considering kinetic energy only because the volume of the low desity particle is relatively large, thus it has a larger footprint when landing on the target, thereby causing a larger crater at the surface.

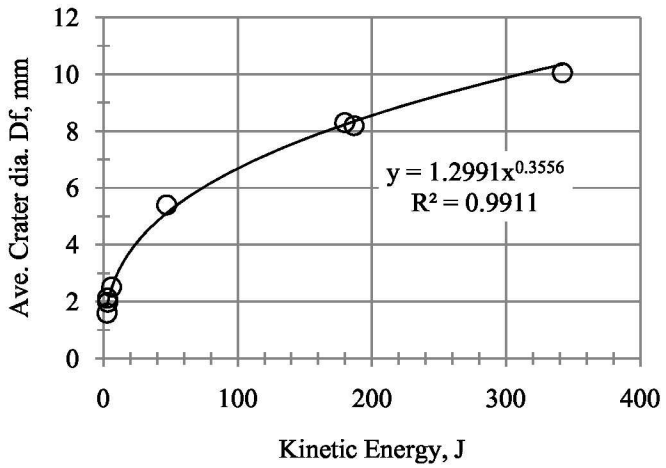

Figure 7. Average Crater Surface Diameter in Aluminum from Projectiles of Different Kinetic Energy. Velocity ranged from 7.5 to 8.34 km/s; target and projectile materials were 6061 T651 and 2017 T4 aluminum respectively; projectile diameters ranged from 0.4 to 1.6 mm. These data yield $D_f = 1.3KE^{0.3556}$.

If we consider Eq(1), and substitue $KE = mV^2/2 = \pi d^3V^2\rho/12$, we get:

$$D_f = 1.3(\pi d^3V^2\rho/12)^{0.3556} = 0.807(d^{1.067}V^{0.71}\rho^{0.3556}) \qquad (4).$$

These powers of d, V, and ρ are frequently seen in the literature and are a direct result of the assumption that kinetic energy controls the level of damage to the target. The units of D_f, d, V, and ρ in Eq.(4) are mm, m, m/s, and kg/m^3 respectively. Kinetic energy is an excellent starting point when building relations between projectiles and resulting damage, however, we believe improvements can be made in assessing the surface diameter of craters by emperically tuning the exponents of d, V, and ρ. We are currently engaged in aquiring additional data to fine tune these exponents. The results presented in this paper use Eq.(1), (2), and (3) to estimate the crater's average suface diameter at given kinetic energies.

We can also estimate crater diameter using Cour-Palais depth of penetration relations and the approximation that the crater diameter is double the crater's depth:[29]

$$D_{f|C\text{-}P} = 2 \times 5.24H^{-0.25}d^{19/18}(\rho_p/\rho_t)^{0.5}(V_n/C)^{2/3}$$

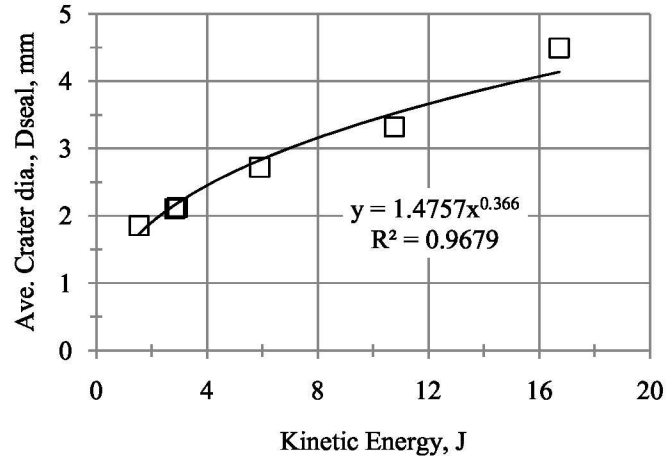

Figure 8. Average Crater Surface Diameter in Parker 0S383-70 from Projectiles of Different Kinetic Energy. Hits more than 25% of the seal width away from the center-line, and hits at low temperatures omitted. Data included is shown in gray in Table 3. These data yield $D_{seal} = 1.476KE^{0.366}$.

where $D_{fC\text{-}P}$ is in cm, H is the Brinell hardness of the target, V_n is projectile velocity normal to the target, C is the speed of sound in the target, and projectile diameter d is in units of cm. A direct comparison of Eq.(4) and the Cour-Palais depth of penetration relation is illustrated graphically in Figure 10 for a 6061 T6 aluminum target, and 0.1 cm 2017 T4 aluminum projectile. In the velocity range of 7 to 10 km/s, the difference between the current work and Cour-Palais' relation is about 29%. This difference is due in part to differences in how the crater diameters are defined.[30] About half of the difference between the C-P relation and Eq.(4) is due to differences in how the crater diameters are defined. Equation (4) yields the average between the crater's d_{fi} and d_{fo}, while the C-P relation yields a diameter more characteristic of the crater's inner diameter.[29,30]

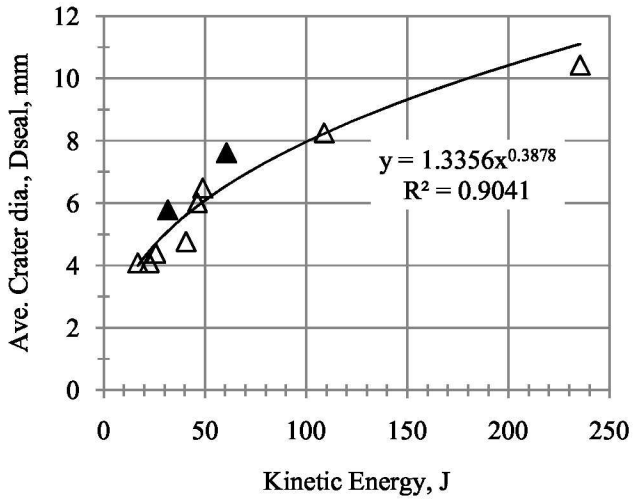

Figure 9. Average Crater Surface Diameter in Esterline ELA-SA-401 from Projectiles of Different Kinetic Energy. Hits more than 25% of the seal width away from the center-line, and hits at low temperatures omitted. Data included is shown in gray in Table 4. The filed triangles indicate Nylon projectiles. These data yield $D_{seal} = 1.336KE^{0.3878}$.

F. BUMPER MMOD Risk Assessments

BUMPER is a risk assessment tool used by NASA.[22] There are many things that BUMPER can be used for and many options and directions one can explore within BUMPER. We use a very specific set of options within BUMPER to determine the cumulative flux of particles of various kinetic energies. This is one step in the solution of MMOD risks to the LIDS seal.

6. *Definition of Failure and Failure Modes*

The LIDS seal is a set of two seals, an inner seal and an outer seal. These seals mate to corresponding metal flange areas on either ISS, or the lunar capsule known as Altair, for example. Thus there are four sealing surfaces whenever the LIDS seal system is mated, two elastomer seals mating to two metal flange areas. Damage to any one of these four surfaces is a potential threat to the LIDS system. For this seal design, failure occurs when one or more of the following set of failures occurs:

a) The inner and outer seals fail, the probability of which is defined as P(Sio);

b) The inner seal and outer flange areas fail to seal, the probability of which is defined as P(SiFo);

c) The outer seal and inner flange area fail to seal, the probability of which is defined as P(SoFi);

d) The inner and outer flange areas fail to seal, the probability of which is defined as P(Fio).

Each one of these failures is a combination of two failures. A failure in both an inner seal or flange AND an outer seal or flange must occur for the system to fail. Thus the probability associated with each of the failure modes noted above is an intersection of two failures (both must occur). The probability of the LIDS seal system to fail is then the union of these intersecting failure modes. The seal and flange areas have different flight histories which are incorporated into BUMPER. Once the probability of failure for the seals and flange areas are found, the appropriate intersections and then unions are determined, thus yielding the probability of seal failure for a particular mission.

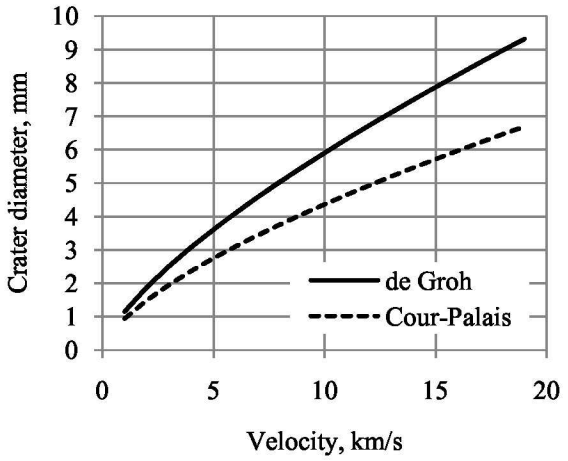

Figure 10. Comparison of the Cour-Palais and de Groh's Eq.(4). Comparison employs 6061 T6 target, and 2017 T4 0.1 cm diameter aluminum projectile.

7. BUMPER results and data processing

Table 5 presents an example of BUMPER inputs and outputs and some of the data processing that was done to estimate MMOD risks to the LIDS seal. The example is for the case of Parker seal flange areas on ISS after a period of 2 years with Node 2 facing forward, into the orbital velocity vector of ISS (ram facing LEO exposure). This case by its self provides a good estimate of MMOD risk for a mission to ISS after the flange has been in place on ISS for 4 years, since docking nodes on ISS are covered about half of the time and because contributions to risk from this area are much greater than all others combined. Risks from this area are relatively large because the MMOD flux is high for the forward facing ram orientation. Figure 11 shows how the probability of a seal failure accumulates for the inner and outer flange areas. Contributions to risk are small at high kinetic energies because the population of

Table 5. BUMPER Results and Data Processing Example. BUMPER results and partial data processing for Parker flange areas exposed to LEO for 2 years. Kinetic energy, KE, is input into BUMPER which determines the cumulative Probability of Impact (PoI), SumPoI, for the inner and outer flange areas; the PoI for a Single KE is found by subtracting off the PoI for the next larger KE (Single $PoI_i = SumPoI_i - SumPoI_{i+1}$); Single $KE_i = (KE_i + KE_{i+1})/2$; $W_F = D_f - D_{crit} = 1.3KE^{0.3556} - 1.3KE_{crit}^{0.3556}$, where KE_{crit} is found by experiments to be 2.9 J in this case; W is the seal area width; the probability of a seal failure at a particular projectile energy is Single PoI x W_F/W; the cumulative probability of seal failure at a particular kinetic energy or greater is found by summing the Single PoF values ($SumPoF_i = SumPoF_{i-1}$ + Single PoF_i). Single KE and SumPoF are plotted in Figure 11.

KE	Sum PoI	Sum PoI	Single KE	Single PoI	Single PoI	W_F	Width Ratio	Single PoF	Single PoF	Sum PoF	Sum PoF
J	Inner	Outer	J	Inner	Outer	mm	W_F/W	Inner	Outer	Inner	Outer
2	9.6E-02	9.8E-02	2.44	2.9E-02	2.9E-02	0	0	0	0	2.8E-03	2.8E-03
2.88	6.7E-02	6.9E-02	2.94	2.7E-03	2.7E-03	0	0	0	0	2.8E-03	2.8E-03
3	6.5E-02	6.6E-02	3.25	9.3E-03	9.5E-03	0.023	0.001	1.1E-05	1.2E-05	2.8E-03	2.8E-03
3.5	5.5E-02	5.7E-02	3.75	7.1E-03	7.2E-03	0.132	0.007	4.9E-05	5.0E-05	2.8E-03	2.8E-03
4	4.8E-02	5.0E-02	4.3	6.5E-03	6.7E-03	0.232	0.012	7.9E-05	8.1E-05	2.7E-03	2.8E-03
4.6	4.2E-02	4.3E-02	4.9	5.0E-03	5.2E-03	0.341	0.018	9.0E-05	9.3E-05	2.6E-03	2.7E-03
5.2	3.7E-02	3.8E-02	5.6	5.2E-03	5.3E-03	0.442	0.023	1.2E-04	1.2E-04	2.5E-03	2.6E-03
6	3.2E-02	3.3E-02	7	8.5E-03	8.7E-03	0.565	0.030	2.5E-04	2.6E-04	2.4E-03	2.5E-03
8.0	2.3E-02	2.4E-02	9	5.1E-03	5.2E-03	0.832	0.044	2.2E-04	2.3E-04	2.2E-03	2.2E-03
10	1.8E-02	1.9E-02	12.5	6.7E-03	6.9E-03	1.059	0.056	3.7E-04	3.8E-04	1.9E-03	2.0E-03
15.0	1.1E-02	1.2E-02	17.5	3.3E-03	3.4E-03	1.520	0.080	2.6E-04	2.7E-04	1.6E-03	1.6E-03
20	8.2E-03	8.4E-03	25	3.2E-03	3.2E-03	1.890	0.099	3.1E-04	3.2E-04	1.3E-03	1.4E-03
30.0	5.1E-03	5.2E-03	35	1.5E-03	1.5E-03	2.479	0.130	1.9E-04	2.0E-04	1.0E-03	1.0E-03
40.0	3.6E-03	3.7E-03	70	2.4E-03	2.5E-03	2.952	0.155	3.7E-04	3.8E-04	8.1E-04	8.3E-04
100	1.2E-03	1.2E-03	125	4.2E-04	4.4E-04	4.824	0.253	1.1E-04	1.1E-04	4.4E-04	4.5E-04
150	7.3E-04	7.5E-04	171	1.7E-04	1.8E-04	5.868	0.308	5.3E-05	5.4E-05	3.3E-04	3.4E-04
192	5.6E-04	5.8E-04	196	2.5E-05	2.5E-05	6.581	0.345	8.5E-06	8.7E-06	2.8E-04	2.8E-04
200	5.4E-04	5.5E-04	215	7.7E-05	7.9E-05	6.705	0.352	2.7E-05	2.8E-05	2.7E-04	2.7E-04
230	4.6E-04	4.7E-04	245	5.9E-05	6.1E-05	7.143	0.375	2.2E-05	2.3E-05	2.4E-04	2.5E-04
260	4.0E-04	4.1E-04	280	6.0E-05	6.2E-05	7.546	0.396	2.4E-05	2.5E-05	2.2E-04	2.2E-04
300	3.4E-04	3.5E-04	350	9.7E-05	1.0E-04	8.040	0.422	4.1E-05	4.2E-05	1.9E-04	2.0E-04
400	2.4E-04	2.5E-04	450	5.7E-05	5.8E-05	9.110	0.478	2.7E-05	2.8E-05	1.5E-04	1.6E-04
500	1.9E-04	1.9E-04	575	5.1E-05	5.2E-05	10.02	0.526	2.7E-05	2.7E-05	1.3E-04	1.3E-04
650	1.4E-04	1.4E-04	725	3.1E-05	3.1E-05	11.18	0.587	1.8E-05	1.8E-05	1.0E-04	1.0E-04
800	1.1E-04	1.1E-04	900	2.6E-05	2.6E-05	12.19	0.640	1.6E-05	1.7E-05	8.2E-05	8.4E-05
1000	8.0E-05	8.2E-05	1200	2.8E-05	2.8E-05	13.35	0.701	1.9E-05	2.0E-05	6.5E-05	6.7E-05
1400	5.2E-05	5.4E-05	1700	1.9E-05	2.0E-05	15.29	0.802	1.5E-05	1.6E-05	4.6E-05	4.7E-05
2000	3.3E-05	3.4E-05		3.3E-05	3.4E-05	17.61	0.924	3.1E-05	3.2E-05	3.1E-05	3.2E-05

these larger, faster particles is less. Contributions to the probability of a seal failure decline and go to zero at the lower kinetic energies because the ratio W_F/W is becoming small, and particles below 2.9 J do not cause seal failure in this case. The major result of this example is the maximum SumPoF values, found at the top of the SumPoF columns in Table 5, and in the upper left of Figure 11. By multiplying these two SumPoF values we determine the intersection of the probabilities of a MMOD failure for the inner and outer flange areas (failure mode "d" noted above).

The contributions to risk from the different failure modes and their union is presented in Figure 12 for the 2 year Parker case; shown are the probabilities of seal failure caused by MMOD damage to: both seals, P(Sio); the inner seal and outer flange area, P(SiFo); the outer seal and inner flange area, P(SoFi); both flange areas, P(Fio); and their union, the total probability of failure for this case, PoF = P(Sio) + P(SiFo) + P(SoFi) + P(Fio).

Figure 13 presents MMOD risk estimates, PoF, for the LIDS seal and flange system for the two elastomers for various mission times and flight altitudes. Details relevant to these cases are:

- 0.01 years: Represents threats to CEV during the approximately 4 day period between launch and docking with ISS or Altair.
- 0.02 years: Reflects risk to Altair during the approximately 8 day period after launch, and before docking with CEV. This includes risks to CEV.
- 0.58 years: MMOD risks during a 217 day Lunar mission assuming the seal and Altair flange are exposed the whole time. Includes the 4 and 8 day LEO periods for CEV and Altair respectively.
- 1 year: Probability of failure upon docking to ISS after 1 year of ram exposure at Node 2. Includes 4 days of CEV seal exposure, and is representative of the level of risk expected for an ISS flange in service for 2 years since docking nodes are exposed only half of the time.

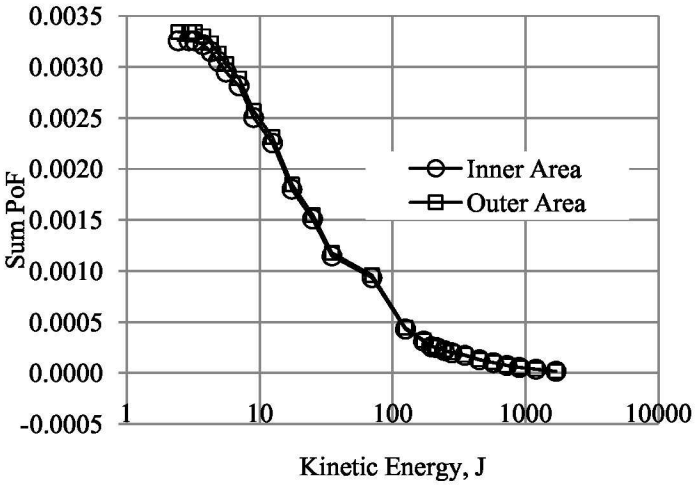

Figure 11. Cumulative Probability of Parker Flange Area Failure. Data presented in Table 5; 2 years LEO ram facing exposure. The contribution to risk from the flange areas failing would be the intersection of both the inner and outer areas failing, P(Fio) = 3.26E-3 x 3.34E-3 = 1.09E-5, shown in Figure 12. This risk intersection is then summed with contributions from other failure modes.

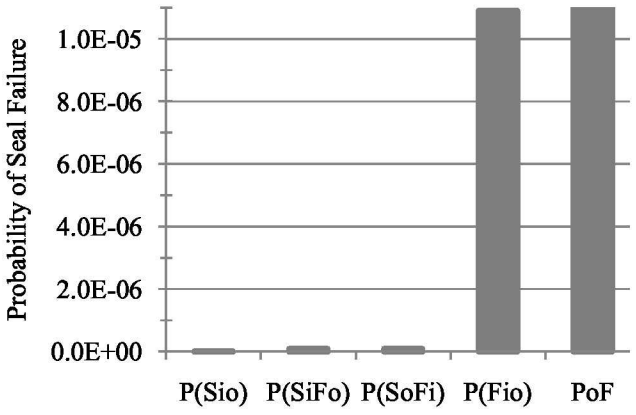

Figure 12. Probability of Failure for the Four Failure Modes and their Union, PoF. Data for the Parker, 2 year mission to ISS case, with Parker flange data from Table 5 and Figure 11. Shown are the probabilities of seal failure caused by MMOD damage to: both seals, P(Sio); the inner seal and outer flange area, P(SiFo); the outer seal and inner flange area, P(SoFi); both flange areas, P(Fio); and their union, the total probability of failure for this case, PoF = P(Sio) + P(SiFo) + P(SoFi) + P(Fio). Risks to the flange areas, P(Fio), dominate.

- 2 year: PoF for a mission to ISS resulting from 2 years of ram exposure at Node 2; representative of risks due to 4 years of flange service at Node 2; includes 4 days of CEV LEO exposure.
- 5 years: PoF for a mission to ISS after Node 2 has received 5 years of ram exposure. Includes 4 days of CEV seal exposure. It is expected to take 10 years to accumulate this level of MMOD exposure.
- 10 years: PoF for a mission to ISS after 10 years of ram exposure at Node 2; includes risk to CEV's LIDS seals. It is expected to take 20 years to accumulate this level of MMOD exposure

Figure 13 shows that threats to the Esterline seal are much lower compared to the narrower Parker seal. Note that the scale in Figure 13 is logarithmic; the probability of failure of the Esterline seal is between 2 and 3 orders of magnitude less than the Parker seal. This is because the Esterline seal is wider, thus requires a more energetic particle (bigger and or faster) to causes its failure. Such larger particles are less frequent is space.

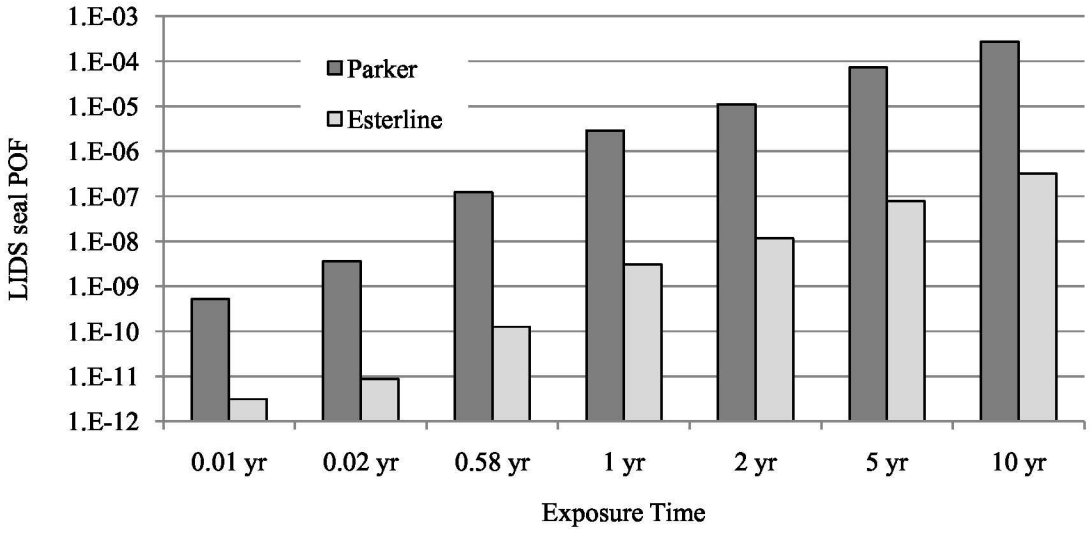

Figure 13. Probability of Failure due to MMOD for Parker and Esterline LIDS seal designs. Mission times reflect threats to CEV prior to docking, CEV docking with Altair, full exposure during a Lunar mission, and missions to ISS after 1, 2, 5, and 10 years of ram exposure at Node 2.

8. Comparison of Allowed Risk to Expected Risk

In the 1990's the International Space Station Project developed the formula:

$$PNP = PNF = X^{A*t} \qquad (5)$$

to allocate MMOD risks to vehicles and modules docked to ISS. PNP is Probability of No Penetration, X is a constant, A is the area exposed to the MMOD environment for the item being considered in square meters, and t is time of the exposure in years. Since failure occurs at penetration, PNP is analogous to PNF, Probability of No Failure. NASA determines an acceptable level of risk (PNF) for a particular vehicle area (A), time period (t), and failure mode (such as Loss of Crew, or Loss of Mission). With PNF, A, and t defined, the constant X is determined for the case being considered. With this scenario specific X, the allowable risks associated with smaller portions of the vehicle and mission can be determined. This assumes the risk is spread evenly over the whole area, A. The MMOD risks to each of these smaller areas of the vehicle is considered and compared to its allotted portion found using Eq. (5). In this way, sections of the vehicle or mission that present the highest risk can be found.

Sometimes, certain sections of a vehicle are given a specific MMOD risk sub-allotment. For such cases, acceptable levels of risk are defined and X values determined which are unique to a specific section of the larger vehicle. The LIDS system has been given such a sub-allotment, and allowable MMOD risk levels defined for Loss of Mission objective (LOMo) failures during ISS, Lunar Sortie and Lunar Outpost missions. Table 6 shows the programmatically set allowable risk of LOMo due to MMOD damage to LIDS, a preliminary estimate of LIDS

surface area over which this level of risk is shared, and the time considered for each mission. With PNF, A, and t defined, X for the LIDS system is found and used to determine allowable levels of risk (PNF) to the LIDS seal for each mission, assuming uniform proportioning of MMOD risk over all of LIDS's areas. The LIDS area listed in Table 6 (7.23 m^2) was found by FEM modeling of external as well as internal LIDS elements. The applicability of this area to our case is still being considered. Internal surface areas within LIDS are exposed to a lesser extent than the outside of LIDS, thus we consider this area to be a very conservative (high) estimate. Area estimates of LIDS based on its overall structure, including both internal and external surfaces composing the "pressure vessel" yields an area of 4.3 m^2. Using a lesser area such as 4.3 m^2 would result in lower X values, and a lower PNF requirements for the LIDS seal. Comparing MMOD risk estimates from BUMPER to allowed levels shows whether the seal is expected to consume more, or less, than its fair share of available risk. At this time standard CEV mission times are defined as 210 days for ISS and Lunar Outpost missions, and 31 days for Lunar Sortie. It is recognized the X values presented in Table 6 are conservative for the following reasons: 1) refinements are being examined that are expected to reduce the 7.23 m^2 area currently used, and 2) because LIDS is docked for most of the 0.575 year duration of ISS missions only the outer area is exposed to MMOD threats.

Table 6. LIDS system X values for missions, and LIDS Seal Risk Allotment. Shown are the missions considered; allowable levels of risk due to MMOD threats to LIDS programmatically defined; PNP = 1-(1/risk), total area of LIDS (this area is our current best estimate of the LIDS surface area exposed to MMOD threats); time span of exposure; and resulting X values for the LIDS system. Eq.(4) is used with the mission time, X, and LIDS seal area to determine allotted risk to the LIDS seal for a Loss of Mission failure.

Mission	Allowable Risk of LOMo	LIDS PNP	LIDS Area, m^2	Time, years	X	LIDS seal area, m^2	LIDS seal PNF
ISS	1 in 2000	0.9995	7.23	0.5749487	0.99987969	0.172	0.999988102
Lunar Sortie	1 in 33,333	0.99997	7.23	0.0848734	0.99995111	0.172	0.999999286
Lunar Outpost	1 in 33,333	0.99997	7.23	0.5749487	0.99999278	0.172	0.999999286

Figure 14 compares the allotted risk provided to the LIDS seal for a mission to ISS (from Table 6) to the estimates of risk due to MMOD threats to the 2.5 mm wide Parker seal found using BUMPER simulations. For any mission to ISS, the allotment is the same; however, missions to ISS are expected for the next 10 years. When determining the actual risk, the total time sensitive sealing surfaces are exposed to MMOD threats needs to be accounted for. For example, after the flange side of LIDS is placed onto one of ISS's docking nodes for the first time, it will likely sit there and wait for the next spacecraft. The next spacecraft is expected in about six months and when it docks to ISS it will mate with a LIDS flange that has been exposed to space for about half a year. Over the next five years spacecrafts are expected to alternate their dockings between Node 1 and 2, thus after five years, ram exposure at Node 2 is expected to be about 2.5 years (since it has been covered due to previous dockings for half of the five years). As time in orbit accumulates, a strike by a damaging projectile becomes more likely, thus the probability of no failure decreases, while our allowed risk remains the same, as shown in Figure 14.

To satisfy the risk requirement, the expected risks to the seal have to be less than the allocation; put another way, the expected probability of no failure for the seal has to be greater than the PNF allotment. As can be seen in Figure 14, the Parker 2.5 mm wide seal design satisfies risk requirements for service periods of two years or less. Expected risks to the Parker seal are approximately equal to the allotment after five years, and after ten years, the PNF for the Parker seal drops below the risk allotment, thus the 2.5 mm wide Parker seal fails to meet safety requirements after five years of total time in service. Probability of no failure estimates for the Esterline seal were above the PNF allocation for all service periods.

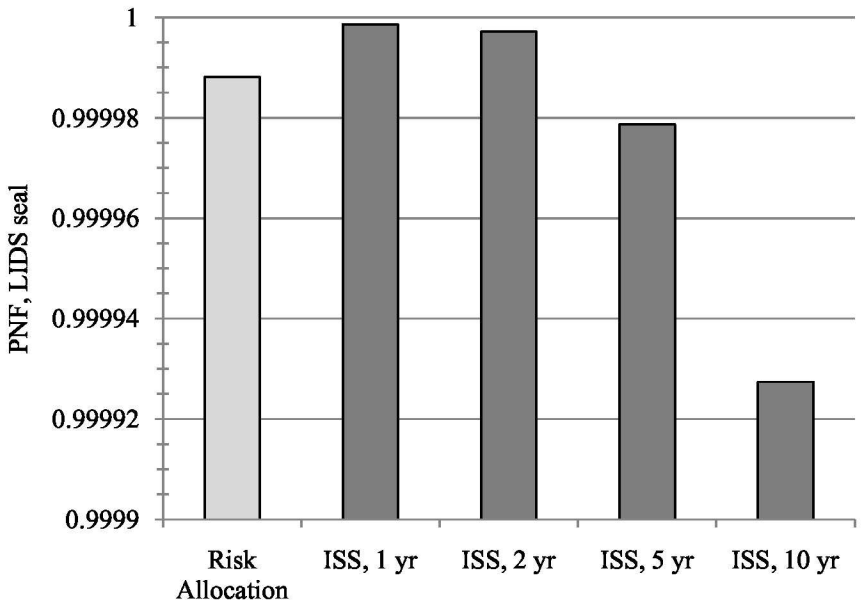

Figure 14. ISS mission MMOD risk allocation compared to expected risk to 2.5 mm wide Parker seal. Risk allocation from Table 6 for a 210 day mission to ISS; risk of seal failure due to MMOD damage shown for total time the ISS side of LIDS has been in service. It is assumed that over this total time in service each docking node has been covered half the time.

Another way to assess MMOD risks to the LIDS seal is to acknowledge the dominance of the ISS side of LIDS, sometimes referred to as the passive side of LIDS, which is on the docking/connecting tube known as ATLAS (APAS To Low impact docking system Adaptor System, where APAS is the Androgynous Peripheral Attachment System). As shown in Figure 12, MMOD risks to the LIDS system are dominated by risks to the ISS flange, P(Fio), since the exposure time for the flange is much greater than the exposure time for the elastomer seals on CEV. The ISS side of LIDS is attached to ISS, so perhaps we should consider LOMo allotments associated with ISS rather than CEV. There is no official LOMo allotment for ISS, however allocation of MMOD threats to ISS for the more restrictive Loss of Crew (LOC) condition has been previously defined as:

$$PNP = 0.99999^{At} \qquad (6)$$

Applying the times of one through ten years, and the LIDS seal area we can solve for a series of LIDS flange MMOD risk allocations; these are shown in Figure 15 with the results for expected MMOD risks to the 2.5 mm wide Parker seal (also shown in Figure14). The current Parker seal design does not meet expected ISS LOC safety requirements after 2 years; LOMo risk allotments are expected to be less stringent.

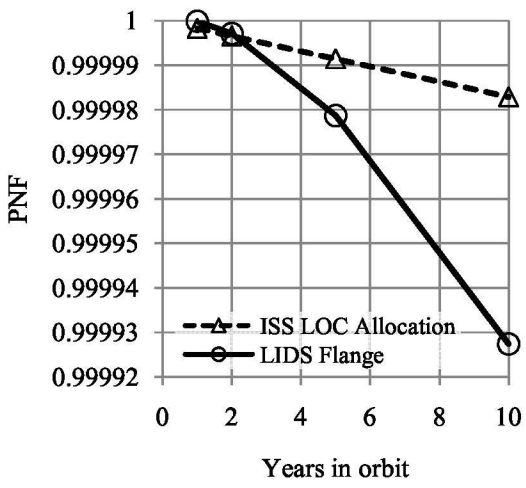

Figure 15. ISS LOC allocation compared to expected risk to the Parker seal. ISS allocation is based on Loss of Crew failure condition, PNF = 0.99999^{At} ; expected MMOD risks to the Parker flange sealing with the 2.5 mm wide seal for total time in orbit; for example, over 10 years, the ISS flange has received 5 years of ram LEO exposure.

9. MMOD risk mitigation

The initial 2.5 mm wide design of the Parker seal was the result of many engineering considerations, one being the clamping load required to adequately compress the seal during docking. Since the 2.5 mm wide seal does not meet desired MMOD safety requirements for in-service times greater than about 3 years, a second look at its width

is warranted since increasing the width will lower expected MMOD risk (raise its PNF). Other options to lower risks from MMOD are to add a third seal, or to add features to the seal so that a leak would not be able to run around the entire circumferential space between the inner and outer seal. From a flight testing and qualification standpoint, the simpler solution is to widen the seal bulb, thus this option will be considered here.

Based on the data in Table 2 and Eq.1 (KE_{crit} = 2.9 J) the critical crater diameter for the flange area with the 2.5 mm wide Parker seal was $D_{crit|f}$ = 2.0 mm, which is 80% of the width of the seal's elastomer bulb, w_{bulb}. If we assume a wider seal will fail at a similar crater-to-seal bulb width ratio, W_F can be defined as $W_{F|f} = D_f - (80\% w_{bulb})$. Table 3 and Eq.(2) indicate the 2.5 mm wide seal fails at a $D_{crit|s}$ = 2.1 mm, which is 84% of the seal bulb width. We assume a wider Parker seal will fail at a similar crater-to-seal width ratio, thus $W_{F|s} = D_{seal} - (84\% w_{bulb})$. Using these assumptions MMOD threats for a variety of seal widths were found and are presented in Table 7 for the case of 10 years in service (5 years ram exposure at Node 2). A Parker seal 3.6 mm wide would approximately meet LOMo MMOD risk requirements for the LIDS seal. For margin considerations, making the seal 3.8 mm wide would exceed the risk allotment of 1 in 84,050 by approximately 25%; making the seal 4.0 mm wide would exceed the allotment by about 50%. We are presently working on how such wider seals will affect docking loads and how those loads might be mitigated.

Table 7. Risk Allocation and PNF for Alternate Parker Seal Designs. LOMo risk allocation for the LIDS seals for missions to ISS; BUMPER estimates of LIDS seal failures due to MMOD resulting from 10 years of service (5 yr ram exposure) on ISS for Parker seal designs of different widths.

	Risk Allocation	2.5 mm wide	3.6 mm wide	3.8 mm wide	4.0 mm wide
PNF	0.9999881	0.9999274	0.9999875	0.9999902	0.9999925
Risk	1 in 84,050	1 in 13,772	1 in 80,151	1 in 102,000	1 in 133,380

IV. Conclusions

This work presents an initial analysis procedure to predict meteoroid and orbital debris threats to candidate docking seals being considered for LIDS. Presented are the results of the hypervelocity impact testing performed to define the failure criteria of the seal/flange combination in the Low Impact Docking System to be used for the Crew Exploration Vehicle docking to the International Space Station and other potential space vehicles planned for lunar missions. Also presented in this paper are the results of the BUMPER code assessment of the probability of failure of the seal/flange system from MMOD impacts. It was shown that the Parker 2.5 mm wide seal design satisfies risk requirements for service periods of two years or less. However, after five years, the Probability of No Failure for the Parker seal drops below the risk allotment, thus the 2.5 mm wide Parker seal fails to meet safety requirements after five years of total time in service. Probability of No Failure estimates for the wider-pad (9.1 mm) Esterline seal were above the PNF allocation for all service periods. Preliminary calculations show that with some design modification, a Parker seal 3.6 mm wide would approximately meet the Loss Of Mission objective (LOMo) MMOD risk requirements for the LIDS seal. For safety margin considerations, making the seal bulb 3.8 or 4.0 mm wide would exceed the LOMo MMOD LIDS risk allotment of 1 in 84,050 by approximately 25% and 50% respectively.

Further refinements being considered for the current methodology include refinements to the areas exposed to MMOD threats under different docked/undocked conditions, flight times, and orientation scenarios affecting the risk allocation calculations. Future activities also include risk mitigation efforts using modified designs and examining the effects of the temperature extreme of 125 °C. Similar risk assessments using BUMPER are planned so that the estimated risk of failure due to MMOD threats to these modified seal designs can be compared to allowable risk levels.

Acknowledgments

The authors sincerely thank Donald Henderson and Karen Rodriguez: Don and Karen's great team at White Sands Test Facility did all of the hypervelocity impacts used in this work. Michael Bjorkman, Eric Christiansen, Kevin Deighton, and William Bohl were instrumental in sorting out the use and interpretation of BUMPER and its results. We acknowledge the collaboration and contributions of Bruce Steinetz as well, and Richard Rauser and Donald Roth for helpful CT work.

References

[1] Hastings, D., and Garrett, H., *Spacecraft-Environment Interactions*, Cambridge Univ. Press, New York, 1996, pp. 82-95.

[2] Eckart, P., et al., *The Lunar Base Handbook*, McGraw-Hill, 1999, pp. 148, 538.

[3] Cour-Palais, B.G. "Meteoroid environmental model-1969 (near Earth to Lunar surface), Technical Report NASA SP-8013, NASA, 1969.

[4] NASA, "Constellation Program Design Specifications for Natural Environments," CxP 70023 Revision A, 2008, pp. 73.

[5] "An Unprecedented Space Collision" Gina Sunseri and Luis Martinez, ABC News, Feb. 12, 2009, http://abcnews.go.com/Technology/Space/story?id=6859247&page=1

[6] "China Confirms Satellite-killing test" Associated Press, msnbc Jan. 23, 2007, http://www.msnbc.msn.com/id/16757285/

[7] Lewis, J. L., Carroll; M. B., Morales; R. H., Le; T. D., National Aeronautics and Space Administration, Washington, DC, "Androgynous, reconfigurable closed loop feedback controlled low impact docking system with load sensing electromagnet capture system," *U.S. Patent No. 6354540*, (2002).

[8] de Groh, K.K., Banks, B.A., and Smith, D.C., "Environmental Durability Issues for Solar Power Systems in Low Earth Orbit," NASA-TM-106775, 1995.

[9] Daniels, C. C., de Groh III, H. C., Dunlap Jr., et. al., "Characteristics of Elastomer Seals Exposed to Space Environments," 43rd AIAA/ASME/SAE/ASEE Joint Propulsion Conf., AIAA 2007-5741, p. 1-16.

[10] Finkbeiner, J.R., Dunlap Jr., P.H., Steinetz, B.M., Daniels, C.C., "Apollo Seals: A Basis for the Crew Exploration Vehicle Seals" AIAA-2006-5259, presented at the 42nd AIAA/ASME/SAE/ASEE Joint Propulsion Conf. Sacramento CA, 2006; also available as NASA/TM-2006-214372.

[11] Cour-Palais, B.G., et al., "Meteoroid Environment Model-1969, near Earth to Lunar surface." NASA SP-8013, 1969.

[12] Coombs, C.R. et al., "Environment Modeling in Near-Earth Space: Preliminary LDEF Results," LPSC XXIII, Lunar and Planetary Inst., 1992, pp. 247-248.

[13] Kessler, D.J., Reynolds, R.C., and Anz-Meador, P.D., "Orbital Debris Environment for Spacecraft Designed to Operate in Low Earth Orbit," NASA TM-1000471, 1988.

[14] Cour-Palais, B. G., "Hypervelocity impact in metals, glass, and composites," Int. J. Impact Engng. Vol. 5, 1987, pp. 221-237.

[15] Christiansen, E.L., "Shield Sizing Equations," technical memorandum to Distribution, SN3-90-131, Oct. 1990.

[16] Evens, S., et al., "Bounding the risk of crew loss following orbital debris penetration of the International Space Station at assemble stages 1J and 1E," Advances in Space Res., Vol. 34, 2003, pp. 1104-1108.

[17] Lambert, M., "Hypervelocity impacts and damage laws," Adv. Space Res., Vol. 19, No. 2, 1997, pp. 369-378.

[18] Herrmann, W., Wilbeck, J. S., "Review of hypervelocity penetration theories, Int. J. Impact Engng., Vol. 5, 1987, pp. 307-322.

[19] Shanbing, Y., Gengchen, S., Qingming, T., "Experimental laws of cratering for hypervelocity impacts of spherical projectiles into thick target," Int. J. Impact Engng. Vol. 15, No. 1, 1994, pp. 67-77

[20] Watts, A. J., and Atkinson, D., "Dimensional scaling for impact cratering and perforation," Int. J. Impact Engng. Vol. 17, 1995, pp. 925-935.

[21] NASA's Constellation website: http://www.nasa.gov/mission_pages/constellation/main/index.html

[22] Natural Environments Branch, "Constellation Program Design Specification for Natural Environments" CxP 70023, Revision A, Feb. 6, 2008, EV13 Spacecraft and Vehicle Systems Dept., Marshall Space Flight Center, pp. 73-76.

[23] de Groh III, H.C., et al., "Adhesion of Silicone Elastomer Seals for NASA's Crew Exploration Vehicle," NASA/TM-2008-215433, 2008.

[24] Natural Environments Branch, "Constellation Program Design Specification for Natural Environments" CxP 00102, Draft 4R, Dec. 19, 2005, EV13 Spacecraft and Vehicle Systems Dept., Marshall Space Flight Center, pp. 50-53.

[25] Anderson, J. C., Henderson, D. J., and Rodriguez, K. M., ".17-caliber Light Gas Gun Velocity Measurement Uncertainty Analysis," WSTF-IR-1086-001-07, 2007.

[26] Thermo Fisher Scientific, "Thermo Scientific NIST Traceable Particle Size Standards," 9000 Series – Glass Size Standards, 2008.

[27] de Groh III, H.C., and Steinetz, B., "Effects of Hypervelocity Impacts on Silicone Elastomer Seals," AIAA-2009-5249, accepted, AIAA Joint Propulsion Conf., Advanced Seals Session, Denver CO, Aug. 8, 2009.

[28] de Groh III, H.C., Daniels, C., Dunlap, P., and Steinetz, B., "Assessing MMOD Impacts on Seal Performance," NASA/CP-2008-215263/Vol2, pp. 143-165.

[29] Christiansen, E, "Meteoroid/Debris Shielding," TP-2003-210788, 2003, p. 30.

[30] Denardo, P., Summers, J. L., and Nysmith, C. R., "Projectile size effects on hypervelocity impact craters in aluminum," NASA TN D-4067, 1967, p. 4.